AGU PUBLICATIONS

Geophysical Research Letters

RESEARCH LETTER
10.1002/2016GL070820

**Key Points:**
- When a source is known, acoustic waves can be reliably detected in the ionosphere using a VIPIR ionosonde
- A special operating mode was developed to detect acoustic waves in the ionosphere
- Automated programming of VIPIR ionosondes can provide high-quality observations of ionospheric acoustic waves at multiple locations

**Correspondence to:**
J. Mabie,
Justin.Mabie@noaa.gov

**Citation:**
Mabie, J., T. Bullett, P. Moore, and G. Vieira (2016), Identification of rocket-induced acoustic waves in the ionosphere, *Geophys. Res. Lett.*, *43*, 11,024–11,029, doi:10.1002/2016GL070820.

Received 11 AUG 2016
Accepted 6 OCT 2016
Accepted article online 10 OCT 2016
Published online 21 OCT 2016



# Identification of rocket-induced acoustic waves in the ionosphere

**Justin Mabie[1,2], Terence Bullett[1,2], Prentiss Moore[3], and Gerald Vieira[3]**

[1]Cooperative Institute for Research in Environmental Sciences, University of Colorado Boulder, Boulder, Colorado, USA, [2]National Centers for Environmental Information, National Oceanic and Atmospheric Administration, Boulder, Colorado, USA, [3]Wallops Flight Facility, National Aeronautics and Space Administration, Wallops, Virginia, USA

**Abstract** Acoustic waves can create plasma disturbances in the ionosphere, but the number of observations is limited. Large-amplitude acoustic waves generated by energetic sources like large earthquakes and tsunamis are more readily observed than acoustic waves generated by weaker sources. New observations of plasma displacements caused by rocket-generated acoustic waves were made using the Vertically Incident Pulsed Ionospheric Radar (VIPIR), an advanced high-frequency radar. Rocket-induced acoustic waves which are characterized by low amplitudes relative to those induced by more energetic sources can be detected in the ionosphere using the phase data from fixed frequency radar observations of a plasma layer. This work is important for increasing the number and quality of observations of acoustic waves in the ionosphere and could help improve the understanding of energy transport from the lower atmosphere to the thermosphere.

## 1. Introduction

Acoustic waves can propagate from the Earth's surface into the space environment after being generated by a number of source types including earthquakes [*Davies and Baker*, 1965], tsunamis [*Occhipinti et al*., 2013; *Makela et al*., 2011], nuclear detonations [*Kanellakos*, 1967; *McKisic*, 1996], volcanic eruptions [*Roberts et al*., 1982], tropospheric convection and forcing [*Zettergren and Snively*, 2013; *Walterscheid et al*., 2003], tropical cyclones [*Xiao et al*., 2007], lightnings and sprites [*Krishnam Raju et al*., 1981; *Farges and Blanc*, 2010], mine blasts [*Calais et al*., 1998], orographic forcing of tropospheric winds [*Walterscheid and Hickey*, 2005], aurora [*Pasco*, 2012], and rocket launches [*Afraimovich et al*., 2003]. We classify these waves as high-altitude acoustic waves (HAAW) which we define as acoustic waves in the thermosphere that interact with the ionosphere. The most energetic HAAW are generated by sources such as earthquakes, volcanic eruptions, and tsunamis, which usually cannot be forecast but can be identified shortly after they occur.

Previous ionosonde observations of HAAW have been limited to observation of irregularities and multiple stratifications of ionospheric layers seen as deformations in ionogram traces as described by *Maruyama et al*. [2011]. These were large-amplitude acoustic waves generated by earthquakes and tsunamis. The Vertically Incident Pulsed Ionospheric Radar (VIPIR) ionosonde is characterized by increased sensitivity to variations in range of observed plasma, to changes in signal-to-noise ratio (SNR) of ionospheric echoes and to changes in the velocity of ionospheric plasma [*Grubb et al*., 2008]. The result is an improved capability for detection of HAAW.

The NASA Wallops Flight Facility (WFF) hosted two successful International Space Station (ISS) resupply missions in 2014. Approximately 8 min after each launch, HAAW were observed perturbing the *F* region of the ionosphere. Detection and identification of these relatively weak, rocket-induced HAAW were aided by knowing the source time and location. We present a description of the observations, the method for detection of HAAW within the data, and a discussion of our results.

## 2. Description of Observations

One Antares rocket was launched from the WFF Mid-Atlantic Regional Spaceport (MARS) on 9 January 2014 at 18:07:05 UTC (henceforth $T+0$ s denoting zero seconds after launch). The rocket was carrying the Orbital Sciences Cygnus 2 spacecraft known as Orb-1. The VIPIR located at the WFF main base was used to observe disturbances in the *F* region of the ionosphere during the Antares flight.

The VIPIR radar is capable of operating simultaneously in both sweep and fixed frequency modes. Sweep frequency mode is the normal operating mode of the WFF VIPIR where observations are made beginning at 1 MHz increasing to 20 MHz during the 50 s observation period. Data are scaled by the Dynasonde software using the NeXtYZ ionogram inversion procedure [*Zabotin et al*., 2006]. In fixed frequency mode the radar makes many observations at one or more frequencies whereby limiting the number of frequencies more observations are made at each one. The observations presented in this letter were made in "shuffle" mode where fixed frequency and sweep frequency observations are interleaved in time by the radar. This allows us to leverage the capabilities of the Dynasonde software while making observations of transient plasma disturbances.

Observations are made with radio frequencies greater than the minimum observable frequency ($f_{\min}$) and less than the peak plasma frequency of the ionosphere ($f_xF_2$). The ionosphere exhibits strong diurnal and seasonal variations in $f_{\min}$ and $f_xF_2$ in addition to variability induced by space weather. Because of these effects, it was necessary to perform a forecast of ionospheric conditions before making fixed frequency observations of the bottomside *F* region. Several days prior to the experiment, climatology and persistence of $f_{\min}$ and $f_xF_2$ were evaluated to determine a set of possible observation frequencies. Frequencies that were within legally restricted bands, contained excessive noise, or were likely to interfere with other radio spectrum users were rejected. Several hours prior to launch, current space weather conditions and environmental radio noise were reevaluated to choose a final observation frequency. The VIPIR operated in shuffle mode several hours before and after launch.

Data sets that were used to identify the plasma disturbance created by the HAAW include the following: spacecraft location tracked by NASA radar systems, temperature in the troposphere measured by a NASA radiosonde, temperature in the middle and upper atmosphere computed by the Mass Spectrometer and Incoherent Scatter Extended 90 model (MSIS-E-90) [*Hedin*, 1991], and the altitude of plasma echoes computed by the Dynasonde software [*Zabotin et al*., 2006].

## 3. Identification of HAAW in VIPIR Data

The acoustic wave source of interest is the ignition of the Antares rocket engines. At $T+12$ s the rocket cleared the launch pad sufficiently that acoustic energy produced by the engines was reverberating off of the ground. At that time the VIPIR was operating in shuffle mode with a fixed frequency of 4165 kHz corresponding to 170 km altitude. To estimate the time for an acoustic wave to propagate from the ground to 170 km altitude, the altitude-dependent sound speed $C_{(z)}$ is computed:

$$C_{(z)} = \sqrt{RT\frac{C_p}{C_v}} \tag{1}$$

where $C_p$ and $C_v$ are specific heats at constant pressure and volume, $R$ is the ideal gas constant, and $T$ is absolute temperature. The propagation time was computed numerically using

$$t = \sum_{h=0}^{h=170\ \mathrm{km}} \frac{dh}{C_{(z)}} \tag{2}$$

where the step size in altitude (d$h$) for each temperature value was chosen to be 1 km.

The predicted time for the HAAW to propagate to 170 km altitude is 499 s. If the HAAW could create an observable plasma disturbance, that disturbance should have occurred during the VIPIR observation that began at 18:15 UTC, about 8 min after launch.

Figure 1 shows the sweep frequency mode ionogram at the predicted arrival time of the HAAW at 170 km. In this ionogram there is no clear evidence of irregularities or multiple stratifications of ionospheric layers that would be a classical signature of a HAAW disturbance as described by *Maruyama et al*. [2011]. The apparent absence of these features suggests that any ionospheric disturbance created by an acoustic wave generated by the rocket engines would not likely have been detected using a traditional sweep frequency ionosonde sounding analysis. There is an $E_2$ layer stratification that appears similar to the acoustic wave signature identified by *Maruyama et al*. [2016], but this layer existed before launch and is not associated with the HAAW.

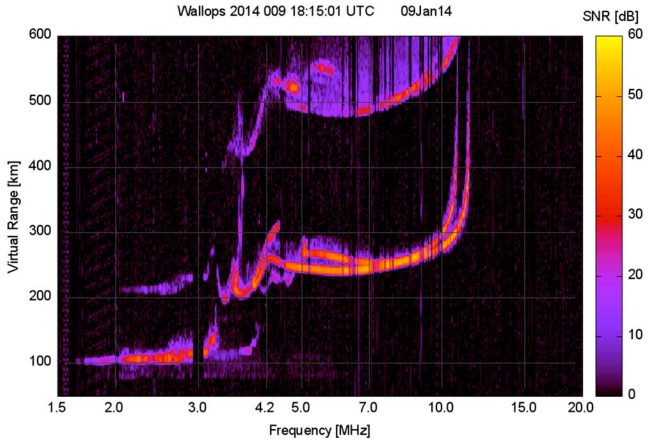


**Figure 1.** The sweep frequency mode ionogram of the observation made when a HAAW is believed to propagate through the *F* region of the ionosphere. This is a plot of the signal-to-noise ratio (SNR) versus radio frequency in megahertz and time of flight scaled in kilometers. The frequency marker at 4.2 MHz provides an approximate reference and context for the fixed frequency observation. Classical HAAW detection would be shown as irregularities and multiple stratifications of ionospheric layers in this plot. Only stratifications of the $E_1$, $E_2$, $F_1$, and $F_2$ layers are present.

There is also a bifurcation of the trace near $f_oF_1$ but that observation was made before arrival of the HAAW at those altitudes.

Figure 2 is the 4165 kHz fixed frequency ionogram of the same observation period shown in Figure 1. The first plasma disturbance is represented as a change in range and intensity of the echoes at $T+504$ s. This is a potential detection of the HAAW generated by ignition of the rocket engines. A second plasma disturbance at $T+520$ s is a potential detection of a HAAW caused by the sonic boom generated during flight.

The ability to detect HAAW using an ionogram is limited because an amplitude-based ionogram is a plot of the intensity of radar echoes as a function of virtual range and time. Virtual range is determined using time of flight of radio waves with resolution being limited to about half the distance a radio wave travels during the VIPIR waveform impulse response. This is about 60 μs corresponding to about 9 km in range, which limits the likelihood of a small plasma displacement being resolved in a VIPIR amplitude-based ionogram. If a plasma disturbance caused by a HAAW is not visible in an ionogram, it may be possible to identify it by analysis of the raw data.

The WFF VIPIR ionosonde makes phase-coherent observations of the electric field of radar echoes with a two-dimensional array of dipole antennas. The radar decomposes the observations into in-phase and quadrature components that allow computation of amplitude and phase path of the echoes. Over many radar pulses a time series of phase path versus time can be constructed. This was done for each pulse by identifying the data point having the largest SNR within a defined range interval. A data set for the observation beginning 18:15 UTC was constructed, and Doppler speeds $V_D$ were computed in the radar line of sight using $c=\lambda f$ so that

$$V_D = \frac{c}{2\pi f}\frac{\partial\Phi(x,y,t)}{\partial t} \tag{3}$$

where $c$ is the speed of light in a vacuum, $f$ is the radio frequency at 4165 kHz, and $\Phi$ is the phase of the received radar echoes as a function of time and horizontal position across the receive antenna array. The 4.2 MHz frequency marker in Figure 1 places the Orb-1 observations near the $F_1$ cusp. This suggests significant radio wave retardation, and the Doppler velocity is expected to differ from the actual plasma velocity depending on the electron density profile.

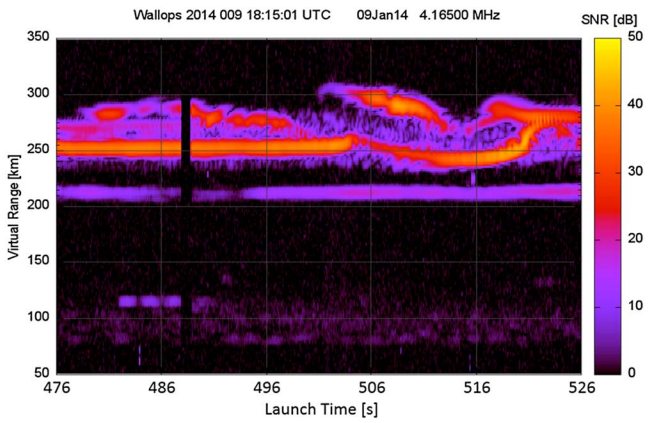


**Figure 2.** A fixed frequency ionogram at 4165 kHz during the Orb-1 flight beginning at $T+476$ s. This plot shows at least three plasma layers including the $E_2$ layer near 210 km virtual range, the $F_1$ layer ordinary mode trace near 250 km virtual range, and $F_1$ layer bifurcated traces near 250 km and 280 km virtual range. Undisturbed plasma is observed at 250 km range (170 km altitude) during the first 27 s. Disturbances occur at $T+504$ s and $T+520$ s. Plasma disturbances are represented in this plot as changes in range and SNR and as bifurcation of the echoes.

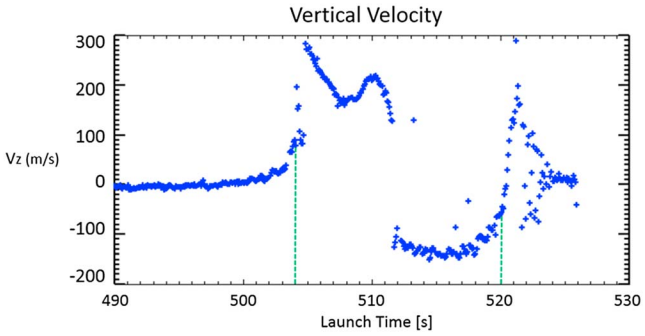


**Figure 3.** Plot of the vertical component of the apparent plasma velocity for the 4165 kHz plasma located near 170 km altitude during the Antares Orb-1 flight. Plasma displacements associated with HAAW wave fronts occur at $T+504$ s and $T+520$ s. The echo source changes near $T+504$, $T+512$, and $T+520$ and different groups of echoes are tracked at these times.

The wave vector of received echoes was computed using a plane wave approximation, and its modulus is defined as

$$|k| = \frac{2\pi f}{c} \tag{4}$$

where the meridional and zonal components are

$$k_x = -\frac{\partial\Phi(x,t)}{\partial x}, k_y = -\frac{\partial\Phi(y,t)}{\partial y} \tag{5}$$

and the vertical component of the wave vector is

$$k_z = \left[\left(\frac{2\pi c}{f}\right)^2 - k_x^2 - k_y^2\right]^{1/2} \tag{6}$$

The Cartesian velocity values are the products of the wave unit vector components and the line of sight velocity.

Figure 3 is a plot of the vertical component of apparent plasma velocity of the echoes with largest SNR after each radar pulse in the 220 km to 320 km range as displayed in Figure 2. Plasma disturbances at $T+504$ s and $T+520$ s are both characterized by a change in the vertical component of plasma velocity. It is this signature that is considered evidence of the passage of the HAAW.

The observation technique was repeated during the Orbital Sciences Cygnus CRS Orb-2 flight on 13 July 2014. Instead of making observations with a single fixed frequency, six fixed frequencies were used. These frequencies and the corresponding real altitudes were 5540 kHz (230.5 km), 5717 kHz (235.8 km), 5899 kHz (241.2 km), 6200 kHz (250.2 km), 6570 kHz (260.8 km), and 6720 kHz (266.3 km). Consistent with the observations made during the Orb-1 flight, a plasma disturbance was observed at the time predicted using equation (2). In this case there was no apparent change in virtual range or SNR of ionospheric echoes, but variations were observed in phase path.

Figure 4 is a plot of the vertical component of apparent plasma velocity beginning approximately 7 min after launch of the Antares Orb-2 rocket. This plot shows plasma displacements at several altitudes caused by a disturbance moving away from the ground. The HAAW disturbances appear as changes in the vertical component of apparent plasma velocity, similar to those observed during the Orb-1 flight.

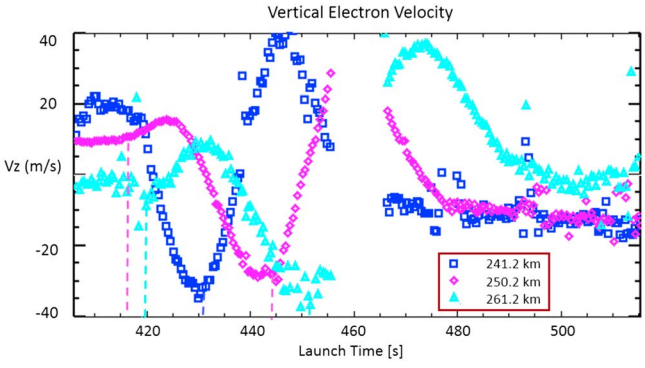


**Figure 4.** Plot of the vertical component of apparent plasma velocity as a function of altitude and time beginning 17:00 UTC on 13 July 2014. Both Antares rockets were physically similar, and the observed differences could be attributed to different atmospheric conditions or by the use of different observation frequencies with respect to $f_xF_2$. Due to radar clock drift introduced by experimental error, there is an uncertainty in observation time of about 1 min.

## 4. Discussion

Plasma disturbances in the ionosphere caused by HAAW vary in magnitude and duration [*Astafyeva et al.*, 2013]. Historically, HAAW-induced ionospheric disturbances have been identified as deformations in ionogram traces [*Maruyama et al.*, 2011]. This historical method limits HAAW identification to those generated by very large events such as strong earthquakes [*Maruyama et al.*, 2012]. HAAW generated by smaller events have been identified using improvements in fixed frequency Doppler sounding techniques [*Artru et al.*, 2004], but these events still had to be relatively large.

Due to the increased number of observations at each frequency, fixed frequency observations like the one demonstrated in Figure 2 can provide for continuous monitoring of plasma displacements which allows for identification of more transient plasma disturbances. For instance, a typical ionosonde will repeat observations at a specific frequency every 1 to 5 min, whereas the observations made during the Orb-1 flight are repeated every 20 ms. Classical detection methods require the ionospheric disturbance to persist long enough to coincide with the observation time, and the disturbance must be large enough to be resolved by the ionosonde. The method presented here can detect relatively small plasma displacements of a few meters per second which persists for as little as a few seconds.

In Figure 2 the disturbances are represented as a change in range on the order of 10 km and SNR of about 20 dB. In Figure 3 the disturbances are displayed as an almost 300 m/s change in apparent vertical velocity. If these disturbances were weaker so that the changes in range, SNR, and vertical velocity were less by an order of magnitude, there would have been no visible signature in the ionogram in Figure 2. However, the change in apparent vertical velocity seen in Figure 3 would still be readily identifiable. For this reason it is necessary to perform analysis of the phase progression of the radar echoes to identify the ionospheric plasma disturbances produced by smaller HAAW.

The results show that the two HAAW observed during the Orb-1 flight propagate with different altitude-dependent speeds. It is known that the sonic boom was generated 75 s after launch near an altitude of 8.26 km. The computational results (equation (2)) place two acoustic waves 40 s apart at this time. At 170 km the disturbances are observed only 17 s apart. This analysis is consistent with the theory that the attenuation rates of HAAW vary and the vertical wave speed differs from the computational result (equation (1)) when the adiabatic invariant potential temperature flux is not conserved [*Schubert et al*., 2005].

HAAW were identified under different atmospheric conditions. Orb-1 was launched midday in January during undisturbed ionospheric conditions, and Orb-2 was launched midday in June during a period of structured ionospheric conditions including the presence of a strong sporadic *E* layer. During the Orb-2 flight, plasma disturbances from a second HAAW were not observed suggesting that one of the acoustic waves may have been attenuated by the atmosphere or had been reflected downward before reaching the observation region. This could be explained by atmospheric conditions [*Artru et al*., 2004] including the observed structure in the ionosphere.

During the Orb-1 flight the plasma response was similar for both HAAW including a rapid change in apparent vertical velocity. The plasma disturbance observed during the Orb-2 flight was characterized by a less abrupt initial change in vertical velocity which increases in intensity over the following half minute.

It is evident that these results are detections of HAAW for several reasons: The observations appear consistent with prior observations and theory; data analysis of the hours prior to and after launch do not indicate the presence of plasma disturbances comparable to the ones that have been identified; the observation times of the disturbances are consistent with computed arrival times for all three HAAW; and variations in observations made under different environmental conditions can be explained using existing theories.

## 5. Conclusions

The plasma disturbances created by rocket-induced HAAW appear to be reliably detectable. The method presented can be used to detect HAAW that are of smaller amplitude than those previously reported. This can be important for understanding energy transport from the lower atmosphere to the thermosphere [*Akmaev*, 2011; *Schubert et al*., 2005; *Rogers and Gardner*, 1980], although we do not attempt to quantify energy transport within this letter.

By using a simple sound speed approximation applied to a known acoustic wave source, it is possible to estimate when and where a HAAW wave front might be located. When the possible location of a HAAW is within the field of view of a VIPIR ionosonde, the resulting plasma disturbance can be observed.

The experimental method developed can be automated when the acoustic wave sources can be identified. With an increasing global distribution of VIPIR sites an automated HAAW detection algorithm would greatly increase the number of HAAW observations which can be used to improve understanding of how they transport energy in the atmosphere.

**Acknowledgments**
This research is supported by NSF grant 1135560. The data used in this research can be obtained through NOAA/NCEI. To obtain a copy of these data, contact ionosonde@noaa.gov. We wish to thank Douglas Drob of the Naval Research Laboratory, Tatiana Sazonova of the Office of the Secretary of the Interior, and Nikolai Zabotin of the University of Colorado for their help in preparing this letter. We also want to thank the NASA Wallops Flight Facility for their continued support of our work and to one of the reviewers for pointing out reference 14.

## References

Afraimovich, E. L., N. P. Perevalova, and S. V. Voyeikov (2003), Traveling wave packets of total electron content disturbances as deduced from global GPS network data, *J. Atmos. Sol. Terr. Phys.*, *65*, 1245–1262, doi:10.1016/j.jastp.2003.08.007.

Akmaev, R. A. (2011), Whole atmosphere modeling: Connecting terrestrial and space weather, *Rev. Geophys.*, *49*, RG4004, doi:10.1029/2011RG000364.

Artru, J., T. Farges, and P. Lognonne (2004), Acoustic waves generated from seismic surface waves: Propagation properties determined from Doppler sounding observations and normal-mode modelling, *Geophys. J. Int.*, *158*, 1067–1077, doi:10.1111/j.1365-246X.2004.02377.x.

Astafyeva, E., S. Shalimov, E. Olshanskaya, and P. Lognonne (2013), Ionospheric response to earthquakes of different magnitudes: Larger quakes perturb the ionosphere stronger and longer, *Geophys. Res. Lett.*, *40*, 1675–1681, doi:10.1002/grl.50398.

Calais, E., J. B. Minster, M. Hofton, and M. Hedlin (1998), Ionospheric signature of surface mine blasts from GPS measurements, *Gephys. J. Int.*, *132*, 191–202, doi:10.1046/j.1365-246x.1998.00438.x.

Davies, K., and D. M. Baker (1965), Ionospheric effects observed around the time of the Alaskan earthquake of March 28, 1964, *J. Geophys. Rev.*, *70*, 2251–2253.

Farges, T., and E. Blanc (2010), Characteristics of infrasound from lightning and sprites near thunderstorm areas, *J. Geophys. Res.*, *115*, A00E31, doi:10.1029/2009JA014700.

Grubb, R. N., R. Livingston, and T. W. Bullett (2008), A new general purpose high performance HF Radar, Proceedings of URSI General Assembly 2008, Chicago, Ill. [Available at http://www.ursi.org/proceedings/procGA08/papers/GHp4.pdf.]

Hedin, A. E. (1991), Extension of the MSIS thermospheric model into the middle and lower atmosphere, *J. Geophys. Res.*, *96*(A2), 1159–1172, doi:10.1029/90JA02125.

Kanellakos, D. (1967), Response of the ionosphere to the passage of acoustic-gravity waves generated by low-altitude nuclear explosions, *J. Geophys. Res.*, *72*, 4559–4576, doi:10.1029/JZ072i017p04559.

Krishnam Raju, D. G., M. Srirama Rao, B. Madhusudana Rao, C. Jogulu, C. Poornachandra Rao, and R. Ramanadham (1981), Infrasonic oscillations in the $F_2$ region associated with severe thunderstorms, *J. Geophys. Res.*, *86*(A7), 5873–5880, doi:10.1029/JA086iA07p05873.

Makela, J. J., et al. (2011), Imaging and modeling the ionospheric airglow response over Hawaii to the tsunami generated by the Tohoku earthquake of 11 March 2011, *Geophys. Res. Lett.*, *38*, L00G02, doi:10.1029/2011GL047860.

Maruyama, T., T. Tsugawa, H. Kato, A. Saito, Y. Otsuka, and M. Nishioka (2011), Ionospheric multiple stratifications and irregularities induced by the 2011 off the Pacific coast of Tohoku Earthquake, *Earth Planets Space*, *63*, 869–873, doi:10.5047/eps.2011.06.008.

Maruyama, T., T. Tsugawa, H. Kato, M. Ishii, and M. Nishioka (2012), Rayleigh wave signature in ionograms induced by strong earthquakes, *J. Geophys. Res.*, *117*, A08306, doi:10.1029/2012JA017952.

Maruyama, T., K. Yusupov, and A. Akchurin (2016), Ionosonde tracking of infrasound wavefronts in the thermosphere launched by seismic waves after the 2010 *M*8.8 Chile earthquake, *J. Geophys. Res. Space Physics*, *121*, 2683–2692, doi:10.1002/2015JA022260.

McKisic, J. M. (1996), Infrasound and the infrasonic monitoring of atmospheric nuclear explosions, Publication of DEPARTMENT OF ENERGY Office of Non-Proliferation and National Security, PL-TR-96-2282.

Occhipinti, G., L. Rolland, P. Lognonne, and S. Watada (2013), From Sumatra 2004 to Tohoku-Oki 2011: The systematic GPS detection of the ionospheric signature induced by tsunamigenic earthquakes, *J. Geophys. Res. Space Physics*, *118*, 1–11, doi:10.1002/jgra.50322.

Pasco, V. P. (2012), Infrasonic waves generated by supersonic auroral arcs, *Geophys. Res. Lett.*, *39*, L19105, doi:10.1029/2012GL053587.

Roberts, D. H., J. A. Klobuchar, P. F. Fougere, and D. H. Hendrickson (1982), A large amplitude traveling ionospheric disturbance produced by the May 18, 1980, explosion of Mount St. Helens, *J. Geophys. Res.*, *87*(A11), 19,037–19,044, doi:10.1029/JA095iA11p19037.

Rogers, P. H., and J. H. Gardner (1980), Propagation of sonic booms in the thermosphere, *J. Acoust. Soc. Am.*, *67*, 78–91.

Schubert, G., M. P. Hickey, and R. L. Waltersheid (2005), Physical processes in acoustic wave heating of the thermosphere, *J. Geophys. Res.*, *110*, D07106, doi:10.1029/2004JD005488.

Walterscheid, R. L., and M. P. Hickey (2005), Acoustic waves generated by gusty flow over hilly terrain, *J. Geophys. Res.*, *110*, A10307, doi:10.1029/2005JA011166.

Walterscheid, R. L., G. Schubert, and D. G. Brinkman (2003), Acoustic waves in the upper mesosphere and lower thermosphere generated by deep tropical convection, *J. Geophys. Res.*, *108*(A11), 1392, doi:10.1029/2003JA010065.

Xiao, Z., S. Xiao, Y. Hao, and D. Zhang (2007), Morphological features of ionospheric response to typhoon, *J. Geophys. Res.*, *112*, A04304, doi:10.1029/2006JA011671.

Zabotin, N. A., J. W. Wright, and G. A. Zhbankov (2006), NeXtYZ: Three-dimensional electron density inversion for dynasonde ionograms, *Radio Sci.*, *41*, RS6S32, doi:10.1029/2005RS003352.

Zettergren, M. D., and J. B. Snively (2013), Ionospheric signatures of acoustic waves generated by transient tropospheric forcing, *Geophys. Res. Lett.*, *40*, 5345–5349, doi:10.1002/2013GL058018.